1 **Ultrasonic degradation of GenX (HFPO-DA) - Performance comparison to**

2 **PFOA and PFOS at high frequencies**

3

4 Nebojša Ilić[a], Afrina Andalib[a], Thomas Lippert[a,e,f], Oliver Knoop[a], Marcus Franke[b,c], Patrick

5 Bräutigam[b,c,d], Jörg E. Drewes[a] , Uwe Hübner[a]

6

7 [a] *Chair of Urban Water Systems Engineering, Technical University of Munich,*

8 *Am Coulombwall 3, 85748 Garching, Germany*

9 [b] *Institute of Technical and Environmental Chemistry, Friedrich Schiller University Jena,*

10 *Philosophenweg 7a, 07743 Jena, Germany*

11 [c] *Center for Energy and Environmental Chemistry (CEEC Jena),*

12 *Philosophenweg 7a, 07743 Jena, Germany*

13 [d] *Fraunhofer IKTS, Fraunhofer Institute for Ceramic Technologies and Systems,*

14 *Michael-Faraday-Straße 1, 07629 Hermsdorf, Germany*

15 [e] *Department of Civil and Environmental Engineering, Northwestern University,*

16 *2145 Sheridan Road, Evanston, IL 60208, USA*

17 [f] *Applied Materials Division, Argonne National Laboratory,*

18 *9700 S. Cass Avenue, Lemont, IL 60439, USA*

19 *\* Corresponding author:*

20 Uwe Hübner*, Chair of Urban Water Systems Engineering, Technical University of Munich,*

21 *Am Coulombwall 3, 85748 Garching, Germany*

22 Phone: + 49 89 289 13706; Fax: +49 89 289 13718; E-mail: u.huebner@tum.de

## 23    Abstract

24    Sonolytic degradation kinetics of hexafluoropropylene oxide-dimer acid (HFPO-DA or GenX)
25    were studied for the first time at four high ultrasonic frequencies (375, 580, 860 and 1,140 kHz)
26    and three power densities (200, 300 and 400 W/L), and compared to the degradation of previously
27    studied perfluorooctanoic acid (PFOA) and perfluorooctanesulfonic acid (PFOS). The frequency
28    of 580 kHz displayed the highest degradation of all three PFAS tested. Within each frequency, the
29    degradation performance increased consistently with increasing power density. Degradation rates
30    were highest for GenX over PFOA to PFOS ($k_{GenX}$ = 0.0501 min$^{-1}$, $k_{PFOA}$ = 0.0444 min$^{-1}$, $k_{PFOS}$
31    0.0153 min$^{-1}$), which is in direct agreement with their reported thermal stability (PFOS > PFOA >
32    GenX). No known by-product formation as expected from the literature on truncation mechanism
33    was detected in the samples (i.e. shorter chain carboxylic acid PFAS). Fluorine mass balance
34    experiments at 580 kHz and 400 W/L confirmed that GenX defluorinated fastest among the three
35    tested PFAS and had lowest loss of fluorine in the mass balance. Degradation experiments with a
36    mixture of all three PFAS displayed lower degradation rates than the individual experiments,
37    where PFOA exhibited the largest reduction in degradation rate (by 31%), followed by GenX (by
38    19%), and finally by PFOS (by 17%). Overall, our study demonstrates that ultrasound can provide
39    effective destruction of different PFAS (70-90% fluorine from mitigated PFAS was detected as
40    inorganic fluoride) with a similar energy demand to alternative PFAS treatment methods reported
41    in literature.

42

43

44    **Keywords:** Cavitation; frequency; GenX; PFAS; sonolysis; ultrasonic treatment

45

## 46    List of Abbreviations

| AOPs | Advanced oxidation processes |
|---|---|
| $E_{EO}$ | Electrical energy per order [kWh/m$^3$] |
| GenX | PFAS technology process name and abbreviation commonly used for HFPO-DA and its ammonium salt |
| HFPO-DA | Hexafluoropropylene oxide dimer acid |
| ISE | Ion-selective electrode |
| LC/MS-MS | Liquid chromatography coupled with tandem mass spectrometry |
| PFAS | Per- and polyfluoroalkyl substances |
| PFOA | Perfluorooctanoic acid |
| PFOS | Perfluorooctanesulfonic acid |
| TISAB | Total ionic strength adjustment buffer |

47

## 1. Introduction

48

49 Per- and polyfluoroalkyl substances (PFAS) are a class of synthetic compounds with a carbon
50 backbone on which the hydrogen is completely (**per**fluoroalkyl substances) or partially
51 (**poly**fluoroalkyl substances) replaced by fluorine atoms[1]. Due to the protective hydrophobic
52 "cloak" around the carbon backbone, PFAS possess features such as water and oil repellency, high
53 chemical stability, higher thermal resistance, etc.[2] Their high mobility in the environment, and
54 persistency towards thermal, chemical, and biological reactions, has caused the accumulation of
55 various PFAS species in humans, animals, and the environment, resulting in the popular name
56 "forever chemicals" for this group of chemicals.

57 Perfluorooctanoic acid (PFOA) and perfluorooctanesulfonic acid (PFOS) were among the first
58 PFAS to be widely used and subsequently regulated[3]. To navigate emerging regulations for PFOA
59 and PFOS, new species of PFAS were introduced by companies in their place. One such
60 replacement came with the GenX process, nowadays used in place of PFOA for manufacturing
61 fluoropolymers such as Teflon. The main chemical of the GenX process, hexafluoropropylene
62 oxide dimer acid (HFPO-DA) and its ammonium salt are commonly referred to as GenX, and often
63 found in water bodies near suspected PFAS point sources[4,5]. Considering that GenX only exists as
64 HFPO-DA in water (salt dissociation), in this work we refer to both HFPO-DA and its ammonium
65 salt as GenX.

66 Several destructive technologies have shown potential for PFAS treatment in the past, from
67 photocatalysis[6], radiolysis[7], and electrochemistry[8,9], to different thermal and non-thermal
68 destructive processes[10] such as ultrasonication, supercritical water oxidation[11], and nonthermal
69 plasma[12]. Regardless, there are currently no destructive processes used at full scale for PFAS
70 treatment, and due to high operational costs, harmful byproduct formation, slow kinetics and/or
71 complexity of effective processes, a hybrid system is likely necessary to minimize the drawbacks
72 and emphasize the strengths of processes in use. To achieve this, a better understanding is needed
73 of where these limitations and strengths of individual processes lie.

74 Ultrasonication represents the acoustic irradiation of a liquid at ultrasonic frequencies (>20 kHz)
75 which induces formation and collapse of bubbles in the liquid (a.k.a. transient cavitation)[13]. The
76 pressure changes in the liquid from the sound wave propagation result in the formation of cavities
77 or microbubbles in the liquid during low pressure events which then proceed to oscillate, growing
78 with each oscillation until they reach the critical radius and eventually undergo a violent collapse[14].
79 These occurring transient adiabatic cavitation events produce localized hot spots with temperatures
80 of 5000 degrees Celsius and pressures of 500 atmospheres in the bubble core[15,16]. The thermal
81 energy generated by this bubble implosion facilitates the decomposition of PFAS molecules that
82 tend to accumulate on the bubble surface due to their amphiphilic nature[17,18]. The thermolysis of
83 PFAS molecules transforms them into their inorganic constituents ($F^-$, $SO_4^{2-}$, CO, and $CO_2$)[19]. In
84 addition, the high temperature and pressure produce the hydroxyl radical (OH•), potentially
85 contributing to the degradation of more susceptible intermediates. The thermolysis induced by
86 bubble implosion events is treated as the key driver of PFAS degradation in this study, considering
87 literature reports that the hydroxyl radical is highly ineffective at PFAS degradation[20,21]. Bubble

88  population density, critical bubble radius, transient collapse temperature, and the PFAS
89  degradation rates are all influenced by sonochemical parameters like the operational ultrasonic
90  frequency[22–24], applied power density[25], shape and design of the reactor, physiochemical properties
91  of dissolved gases and liquid medium, surrounding pressure field in the reactor, and operating
92  temperature[26,27].

93  As discussed in a recent meta-analysis paper by Sidnell et al. (2022)[28], despite over 30 research
94  papers reporting on PFAS degradation with ultrasound, the dependency of degradation
95  performance on sonochemical parameters is still not fully understood. The root cause of this is the
96  lack of common ground for comparison of experimental data. Different concentration ranges,
97  matrix compositions, reactor layout and operational parameters make drawing overarching
98  conclusions from the available studies difficult. As broken down in detail in the meta-analysis, a
99  study by Campbell & Hoffmann (2015)[29] found that PFOA and PFOS degraded most efficiently
100 at 358 kHz between 202, 358, 619, and 1,060 kHz tested (a trend later validated for PFOS by
101 Wood et al. (2019)[30]), and observed an increase in degradation performance when increasing the
102 power density. Two studies by Rodriguez-Freire et al. (2015, 2016)[31,32] examined the effect of two
103 ultrasonic frequencies (500 and 1,000 kHz) on the degradation of PFOS and aqueous firefighting
104 foam mixtures, and reported greater fluoride release and total organic carbon removal at 1,000 kHz
105 (PFAS concentrations not quantified directly). It is important to point out that while Campbell &
106 Hoffmann used a reactor where the PFAS solution is in direct contact with the transducer,
107 Rodriguez-Freire et al. applied differing vessel geometries and reactor volumes (and consequently
108 power density) between frequencies. Such fundamental differences in experimental approaches
109 are likely to affect the propagation of ultrasound and the efficiency of energy transfer into the
110 treated solution, rendering the mentioned studies incomparable. A study by Asakura & Yasuda
111 (2021)[33] reported a strong dependency of sonochemical efficiency on ultrasonic power and
112 frequency, further emphasizing the need for data collection on the topic.

113 This study therefore aims to provide transferable knowledge in ultrasonic degradation of PFAS by
114 investigating the effect that four different high ultrasonic frequencies at several power densities
115 have on the degradation kinetics of three selected PFAS (i.e., GenX, PFOA, and PFOS) by using
116 a reactor with an interchangeable transducer of variable frequency output. The ultrasonic
117 degradation of GenX is reported in this study for the first time. Considering the observations made
118 in previous studies, we conduct all degradation experiments by varying only the output frequency
119 and power, providing a controlled environment that allows us to compare the degradation of the
120 three tested PFAS under identical conditions. Furthermore, we examine the formation of unknown
121 stable fluorinated byproducts at optimal degradation settings with fluorine mass balance
122 experiments.

123 Finally, we propose the use of calorimetric efficiency as a surrogate parameter to normalize the
124 power density applied to the treated solution, since the calorimetric efficiency directly indicates
125 the relative amount of grid energy introduced to the bulk of solution as thermal energy over time.
126 As such, it could prove as a simple to determine reactor parameter that encompasses more difficult
127 to quantify parameters and phenomena that result from varying reactor geometries, distances and
128 solid barriers between transducer and sample, and similar.

## 2. Materials and methods

### 2.1. Consumables

A full list of PFAS chemicals and standards used in this study can be found in Table S5 of the supporting information.

Glacial acetic acid ($CH_3COOH$) and reagent grade sodium chloride (NaCl), as well as LC-MS grade methanol ($CH_3OH$) and 99% formic acid (HCOOH) were acquired from VWR. Fluoride standard solution (1 g/L) was purchased from Sigma-Aldrich. All solutions were prepared with ultrapure water. Thermo Fischer Scientific Orion Star A214 series benchtop pH/ISE meter, Ross Ultra glass combination pH electrode, and 9609BNWP Fluoride Combination Electrode were purchased directly from Thermo Fisher Scientific.

Polypropylene labware was used exclusively in preparation of all experiments and measurements (volumetric flasks, beakers, wide-neck bottles, funnels, pipette tips).

### 2.2. Experimental setup and equipment

For all high-frequency ultrasonic cavitation experiments, a custom reactor manufactured by Meinhardt Ultrasonics (Leipzig, Germany) was used. The experimental setup consisted of a frequency generator, a power amplifier, a 1 L double-walled glass reactor, and two interchangeable transducers to generate different ultrasonic frequencies. A closed loop cooling thermostat LAUDA Alpha RA 8 was used for reactor cooling.

The grid power consumption of the system was measured with a CLM1000 professional plus watt meter (Christ-Elektronik GmbH, Memmingen, Germany). A schematic diagram of the experimental setup and pictures of the reactor can be found in the supporting information (Figures S1 and S2, respectively). All access ports were sealed with silicon caps during the experiments to minimize losses. The frequency signal generator supplies the desired frequency signal to the power amplifier, which amplifies the current and voltage and delivers the signal to the flat transducer attached to the bottom of the glass reactor. The transducer introduced the ultrasound frequency directly to the liquid medium. Both the generator and amplifier were connected to the power grid and one power reading device was used to monitor the actual power that was consumed by both.

### 2.3. Experimental procedures

The cooling thermostat was set to 15 °C throughout the experiments. The PFAS solution was always first kept in the reactor for 15 minutes with the cooling recirculation powered on before starting the ultrasonic transducer. The initial PFAS concentration was always 1 mg/L unless stated otherwise and the pH was adjusted to 7 before starting an experiment. Batch volume was always 500 mL. For the first set of experiments, the degradation kinetics for each PFAS individually (i.e., GenX, PFOA and PFOS) were determined at different frequencies of 375, 580, 860 and 1,140 kHz and power densities of 200, 300 and 400 W/L. Power densities were adjusted by applying the required power on top of a constant idle power of  130 W, i.e., a power reading of 230 W was set

165  for 100 W of active energy input, resulting in a power density input of 200 W/L. The idle power
166  consumption is a property of the reactor system, where the system when turned on but not emitting
167  ultrasonic frequency consumes a constant amount of power (cooling fans, internal electronics).
168  Control experiments without ultrasonic irradiation showed no concentration changes after 90
169  minutes.

170  At predefined time intervals the reactor was shut off for sampling (1.5 mL samples for PFAS
171  quantification) and *in-situ* pH and temperature measurements (done by lowering the temperature
172  and pH probes into the reactor from above). A final sample of 12.5 mL was taken at the end of
173  each experiment and used for quantification of PFAS and inorganic fluoride. Secondly, individual
174  degradation experiments were repeated at 580 kHz and 400 W/L in order to obtain fluoride
175  generation kinetics (by taking 12.5 mL samples at each time interval). Finally, all 3 PFAS were
176  prepared in a single solution where each PFAS had a concentration of 1 mg/L and two experiments
177  were carried out at optimum settings (one with small sample volumes and one with large sample
178  volumes) to compare the degradation and mineralization kinetics of each PFAS in mixture vs
179  individually. Small changes in degradation kinetics that occurred throughout the large sample
180  experiments due to batch volume changes were disregarded and pseudo-first order kinetics were
181  used to obtain kinetic rate constants.

182  The different criteria, objectives and experimental conditions of each experiment type that was
183  conducted are listed in Table S1 of the supporting information.

184  **2.4. Instrumental analysis**

185  PFAS concentrations were quantified using an LC/MS-MS system (Agilent 1260 Infinity,
186  ABSciex Qtrap 5500). The analytical method for this system was developed taking into
187  consideration the German standard method DIN 38407-42, and the US Environmental Protection
188  Agency Method 537.1. A full list of PFAS species included in the analytical method, dilution
189  protocols for the samples, analytical and internal PFAS standards and the full explanation of the
190  analytical method can be found in section 1.4 of the supporting information. A separation column
191  from Waters (XSelect HSS T3, 100 Å, 3.5 µm, 2.1 mm x 100 mm) and the delay column from
192  Agilent (ZORBAX Eclipse plus; C18 95 Å, 3.5 µm, 4.6 mm x 30 mm) were used. The established
193  method had an effective detection range between 5 and 5,000 ng/L. Polypropylene LC vials and
194  polyethylene snap-on caps from Agilent were used in preparation of all LC-MS samples and
195  calibration standards.

196  Free fluoride ions in the extracted samples were measured by using an ion-selective electrode (ISE)
197  and a benchtop pH/ISE meter. Since the experimental samples had low ionic strength that did not
198  contain any Fluoride complexing agents and had fluoride concentrations of less than 0.38 ppm, the
199  low-level Total ionic strength adjustment buffer (TISAB) method from the manufacturer manual
200  was followed. Details about the preparation of the low-level TISAB and the procedure of
201  measuring fluoride ions with ISE can be found in section 1.3 of the supporting information.

202 **2.5. Data analysis and interpretation**

203 **2.5.1. Effect of frequency and power density on physical properties of transient bubbles**
204 Applied power to an ultrasonic transducer is directly proportional to the acoustic intensity, $I$,
205 (which represents the power per unit surface of transducer) and therefore to the acoustic pressure
206 amplitude[34], $P_A$, as presented in equation 1:

207

$$I = \frac{P_A{}^2}{2\rho c} \qquad \text{Equation 1}$$

208

209 Where $\rho$ is the density of the liquid and $c$ is the speed of sound in the liquid. For the purpose of
210 this study, all calculations were done using properties of water as the liquid medium. Higher
211 intensity can generate higher acoustic pressure resulting in an increase in radius, growth speed,
212 and formation rate of the cavitation bubbles[35,36]. The bubble dynamics can also be influenced by
213 the frequency of ultrasound. According to equation 2, the maximum radius of a cavitation bubble
214 $R_{max}$ depends on applied ultrasonic frequency, $\omega_r$, acoustic pressure amplitude, $P_A$ hydrostatic
215 pressure, $P_H$, and density of the liquid, $\rho$, while bubble collapse time, $\tau$ is directly related to the
216 critical radius of bubble, $R_{max}$, pressure in the liquid, $P_m (= P_A + P_H)$, pressure in the bubble, $P_{vg}$,
217 and density of the liquid, $\rho$ (equation 3)[34].

218

$$R_{max} = \frac{4}{3\omega_r}(P_A - P_H)\left(\frac{2}{\rho P_A}\right)^{\frac{1}{2}}\left[1 + \frac{2(P_A - P_H)}{3P_H}\right]^{\frac{1}{3}} \qquad \text{Equation 2}$$

$$\tau = 0.915\, R_{max}\left(\frac{\rho}{P_m}\right)^{\frac{1}{2}}\left(1 + \frac{P_{vg}}{P_m}\right) \qquad \text{Equation 3}$$

219 Based on equations 2 and 3, maximum radius, collapse time, and surface area-volume ratio of
220 bubbles were calculated for all applied frequencies and power densities and are presented in Table
221 1.

222

223

224 **Table 1.** Calculated cavitation bubble properties at all applied ultrasonic frequency and power densities.

| Frequency, $\omega_r$ (kHz) | Applied power density (W/L) | Intensity, I (W/cm$^2$) | Pressure amplitude, $P_A$ (atm) | $R_{max}$ (μm) | Collapse time, $\tau^*$ (μs) | Area-Volume ratio (A/V) (μm$^{-1}$) |
|---|---|---|---|---|---|---|
| **375** | 200 | 2.26 | 2.57 | 10 | 0.48 | 0.30 |
| | 300 | 3.40 | 3.15 | 13.12 | 0.59 | 0.23 |
| | 400 | 4.53 | 3.64 | 15.62 | 0.66 | 0.19 |
| **580** | 200 | 2.26 | 2.57 | 6.48 | 0.31 | 0.46 |
| | 300 | 3.40 | 3.15 | 8.49 | 0.38 | 0.35 |
| | 400 | 4.53 | 3.64 | 10.10 | 0.43 | 0.30 |
| **860** | 200 | 2.26 | 2.57 | 4.37 | 0.21 | 0.69 |
| | 300 | 3.40 | 3.15 | 5.72 | 0.26 | 0.52 |
| | 400 | 4.53 | 3.64 | 6.81 | 0.29 | 0.44 |
| **1140** | 200 | 2.26 | 2.57 | 3.30 | 0.16 | 0.91 |
| | 300 | 3.40 | 3.15 | 4.32 | 0.19 | 0.69 |
| | 400 | 4.53 | 3.64 | 5.14 | 0.22 | 0.58 |

225 *Assuming $P_{vg} = 0$ and there was no influx of gas into the cavity during the growth cycle of the transient bubble.

226 From the calculations we can see that with an increase in frequency, maximum radius and
227 consequently the surface area of a bubble decrease, while the ratio of surface area to volume
228 increases. With a larger maximum radius, the collapse core temperature also increases[16].

229 **2.5.2. Calorimetric efficiency of reactor**
230 Calorimetric measurements were done to quantify the thermal energy introduced to the water by
231 the reactor through cavitation in comparison to the energy consumed from the power grid. To
232 measure the calorimetric efficiency at each operational setting, the reactor was operated for 20
233 minutes with 500 mL of water at each frequency and power setting without cooling. The
234 temperature of the water was measured every minute, while the grid power consumption was
235 logged by the power reading device. After first calculating the introduced thermal energy (i.e.,
236 output power), we compared this energy to the energy consumed by the reactor in the same time
237 frame (i.e., input power including the idle power consumption) and obtained the calorimetric
238 efficiency of the reactor at different frequencies and power settings. For simplicity, we disregarded
239 the heat capacity of the thin glass walls and considered the outer chamber of the reactor an insulator
240 for the system as it is filled with air.

241    The calorimetric energy efficiencies plotted in Figure 1 show that the calorimetric efficiency of
242    the reactor increases with the increase in power density at each frequency, implying a larger
243    relative number of cavitation events per unit time and thus a higher amount of the consumed
244    electrical energy introduced into the system as heat. Unlike power density, frequency does not
245    display a steadily increasing trend, but rather an efficiency maximum at 580 kHz. Data that was
246    obtained experimentally and calculated for the purpose of determining the calorimetric efficiency
247    is provided in Table S11 of the supporting information.
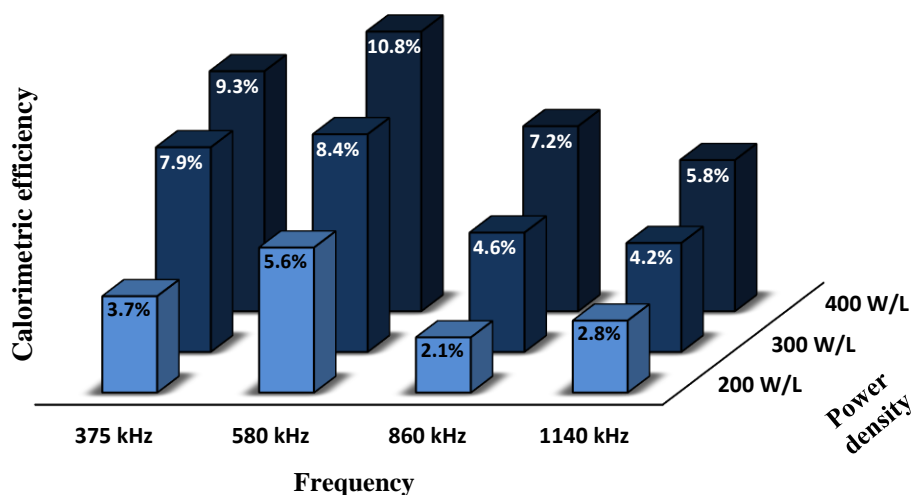


**Figure 1.** Calorimetric energy efficiencies for different frequency and power settings

248

### 2.5.3. Reaction kinetics

250    All three sonochemical degradation profiles for GenX, PFOA and PFOS fit best with a pseudo-
251    first-order kinetics model, depicted in linearized form in equation 4:

$$\ln\left(\frac{c_t}{c_0}\right) = -kt \qquad \text{Equation 4}$$

252    Where $c_t$ indicates the molar concentration of the targeted compound at time $t$, $c_o$ depicts initial
253    concentration and $k$ is the pseudo-first-order rate constant.

254    Slope values and the standard error for the determined degradation rate constants were obtained
255    using the LINEST function in Excel.

256

# 3. Results and discussion

## 3.1. Frequency and input power effect on PFAS degradation kinetics

Figure 2 represents the degradation rate constants from individual degradation experiments for GenX at all frequency and power settings (Figure 2a), as well as the degradation rates for all three PFAS at 580 kHz, the frequency which demonstrated highest degradation of all three PFAS (Figure 2b). Degradation rate constants were obtained using linear regression and the standard errors are displayed. The majority of $R^2$ values varied from 0.97 – 0.99, although with several values in the 0.93-0.97 range, mainly at settings with lower degradation observed. A full overview of the degradation rate constants for each PFAS at all power and frequency settings can be found in Table S12 of the supporting information. The linearized pseudo-first order degradation kinetics plots for each PFAS at varying power density and frequency settings are provided in the SI (Figures S3-S5). It is important to point out that all obtained degradation rates for identification of optimal settings were obtained from single kinetics experiments with a minimum of six data points. There is high certainty from referenced literature that PFAS degradation with ultrasound follows pseudo-first order kinetics. This, together with our experimental design ensuring minimal influence of external factors led us to hypothesize that any replicates would provide very minor deviation in data. A single experiment was conducted in duplicate (PFOA @ 580 kHz & 400 W) to test this hypothesis, where nearly identical degradation performance was observed in both runs, with differing starting concentrations (first order degradation rate is independent of initial concentration, providing further confidence in the models). The duplicate experiment comparison is presented in supporting information Figure S6.
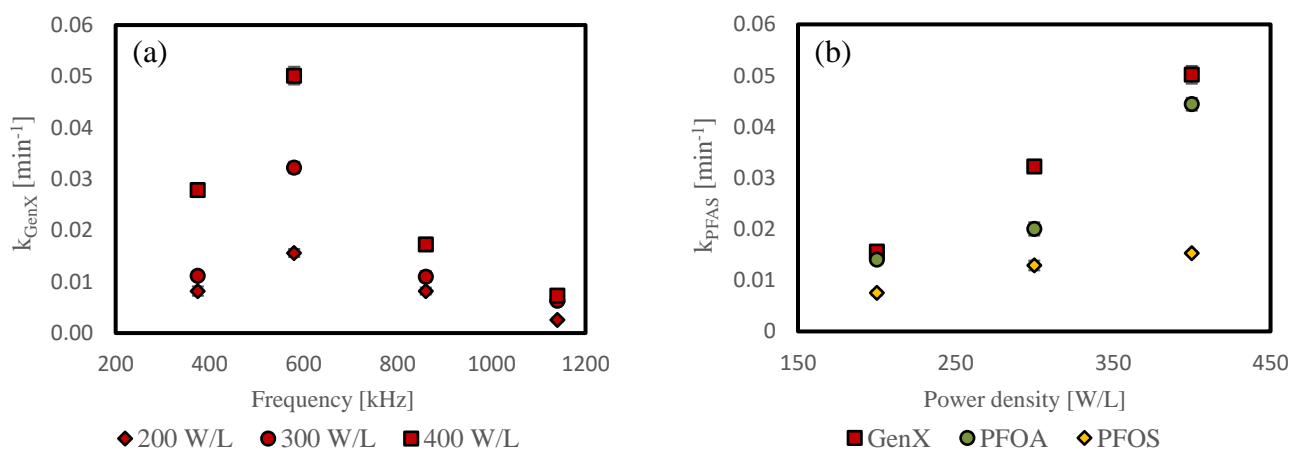


**Figure 2.** Pseudo-first-order kinetic rate constants for (a) GenX at all frequency and power density settings, and (b) all three PFAS at 580 kHz frequency, based on individual degradation experiments. The error bars represent standard errors for the degradation rate constants obtained from the LINEST function in excel. If not visible, calculated error bars were smaller than the corresponding data point symbol.

The degradation rates of PFOA, PFOS, and GenX all followed the same trend and achieved maxima at 580 kHz frequency and 400 W/L power density, highlighting these settings as optimal

285  for PFAS degradation from the ones tested and implying a complex codependence of operational
286  parameters in sonolysis. Independent of frequency, a consistent rise in degradation rate can be
287  noticed with the increase in power density within each single frequency, with a more observable
288  increase at 375 and 580 kHz frequencies. The temperature in the reactor appeared stable
289  throughout every experiment ($\Delta t \approx 1$ °C), and stabilized between 16 - 21 °C depending on the
290  operational parameters. Generally, slightly higher stationary temperatures were observed at
291  operational parameters with higher calorimetric efficiencies. The pH change in experiments
292  corresponded to the observed degradation performance, with the lowest measured pH being 3.6
293  for all 3 PFAS. Temperature measurements, pH values, and fluoride and PFAS concentration data
294  are available for download as an Excel file from the Zenodo repository[37].

### 3.1.1.  Discussion on degradation mechanism

296  Certain wave and bubble properties could explain the observed degradation performance in Figure
297  2. While frequency indicates the number of periods a wave achieves in one second, one period is
298  the time a wave takes to complete one full vibrational cycle (one compression and one rarefaction
299  cycle) and can be derived directly from the frequency. Therefore, one full compression/rarefaction
300  cycle lasts one half-period, or in the case of 1,140 kHz which has a period of 0.88 µs, each of these
301  cycles lasts 0.44 µs. This half-period is significantly shorter than the 1.33 µs half-period (and thus
302  rarefaction cycle) of 375 kHz. The collapse time of a cavitation bubble is also a function of
303  ultrasonic frequency and power, as mentioned above in equation 3 and calculated for all our
304  settings in Table 1, where we see that the bubble collapse time increases with the increase in power
305  input at each frequency. In the case of 1,140 kHz, the collapse time at 400 W/L equals the time
306  between the maximum pressure of the compression cycle and the beginning of a rarefaction cycle
307  (0.22 µs). A greater number of bubbles are therefore presumed to experience stable oscillation, as
308  the next rarefaction cycle begins before the bubble completes the collapse[34,35]. In essence, the
309  bubbles keep oscillating in phase with the rarefaction and compression cycles, growing slowly
310  through rectified diffusion but never undergoing transient collapse, which could explain the
311  significantly reduced performance observed at 1,140 kHz.

312  According to previous findings reported in literature, after the interfacial adsorption of PFAS
313  molecules to the surface of the cavitation bubbles, further degradation occurs via pyrolytic
314  cleavage of the ionic head group from the perfluorinated tail[19,38]. However, not all authors agree
315  on this concept as they observed quite the opposite trend which shows shortening of perfluoro tails
316  as the initial stage of degradation rather than the cleavage of the head group[31,39]. Based solely on
317  the bond dissociation energies, it is more likely that the PFAS degradation begins with headgroup
318  cleavage, since C-F bond energies ($\approx$440-530 KJ/mol)[40] are higher than that of C-C ($\approx$348
319  kJ/mol)[40] or C-S ($\approx$301-355 kJ/mol)[41] bond. In terms of degradation of GenX, it is assumed that
320  the cleavage of distinctly weak C-O and secondary C-F bonds happen first[42]. After headgroup
321  cleavage, literature suggests that further degradation proceeds via one of two mechanisms: (1)
322  repeated oxidation and truncation, which means formation of shorter chain carboxyl PFAS during
323  degradation and (2) immediate thermolysis within the bubble[28]. Shende et al. (2019)[43] opposed
324  this headgroup cleavage theory and suggested that PFAS molecules arrange themselves around
325  bubble interface non-uniformly when the concentration is below critical micelle concentration and
326  would not necessarily undergo headgroup cleavage.

327  As we did not measure $SO_4^{2-}$ concentration we cannot confirm the headgroup cleavage theory.
328  However, we integrated (among a few other) a full series of carboxylic acid PFAS with 3-9 carbons
329  into our LC/MS-MS method (see chapter 1.4 of the supporting information for a full list of
330  compounds tracked) to investigate the first reported mechanism of repeated oxidation and
331  truncation. No formation of shorter chain PFAS was observed in our degradation experiment
332  samples. Considering the high sensitivity of the LC/MS-MS system (5 – 5,000 ng/L), direct
333  injection of sample series without dilution was not possible (due to initial PFAS concentrations of
334  1 mg/L). Regardless, final samples from experimental series were re-measured with lower
335  dilutions for confirmation, and no peaks were standing out from the short-chain PFAS noise
336  signals. This leads us to conclude that the degradation, while it might be initiated via headgroup
337  cleavage, does not propagate via the cleavage-oxidation mechanism suggested thus producing
338  shorter chain carboxyl PFAS, but rather via immediate pyrolysis of parent PFAS and unknown
339  fluorinated species within the bubble.

340  This conclusion is further supported by the trends observed in degradation kinetics of the three
341  PFAS. The degradation rate for all three PFAS reached the peak at 580 kHz frequency and 400
342  W/L power density. Among the three PFAS, GenX displayed the highest while PFOS exhibited
343  the lowest degradation rate. The observed variation in degradation performance at optimal settings
344  is in direct agreement with the literature-reported thermal stability of the three species of PFAS
345  (PFOS > PFOA > GenX)[44], indicating that thermolysis plays a major role in the sonolytic
346  degradation of PFAS. Finally, fluorine mass balances at optimal settings (discussed in more detail
347  in chapter 3.4.) indicate almost immediate release of fluoride from the degraded PFAS. Some loss
348  of fluorine in the mass balance is observed in the data (70-90% of mitigated PFAS detected as
349  inorganic fluoride). Literature reports state that it is unlikely that fluorine losses occur via gas
350  phase[28], but rather remain in solution as unknown and sonolysis-resistant fluorinated species which
351  form due to incomplete pyrolysis of the parent PFAS.

352  While all three PFAS degrade quickest at 580 kHz, we observe 375 kHz as the second-best
353  frequency for PFOS, whereas the 860 kHz frequency acts as the second-best for PFOA. At 375
354  kHz, the bubble population is lower, while bubbles are larger and collapse with higher core
355  temperatures. At 860 kHz, the bubble population is higher, while the bubbles are smaller and
356  collapse with lower core temperatures[16,45]. This aligns with the report by Shende et al.[43], where the
357  authors postulate that diffusion to the bubble interface acts as the rate limiting step in the
358  degradation of PFOS and PFOA, and that due to the higher specificity constant of PFOS (5.84 M$^{-1}$
359  min$^{-1}$) compared to PFOA (0.85 M$^{-1}$min$^{-1}$), the bubble interface has a higher affinity towards
360  PFOS. Therefore, a lower number of active cavity sites with a higher collapse temperature are
361  better suited for PFOS degradation, as is the case with 375 kHz.

362

### 3.1.2. Degradation performance at higher total PFAS concentration

364  A mixture of all three PFAS (1 mg/L each, 3 mg/L total) was treated at 580 kHz and 400 W/L to
365  study how a higher total PFAS concentration affects the degradation kinetics of the PFAS species
366  compared to their individual degradation experiments. A comparison of the degradation rates is

367   displayed in Figure 3. Linearization plots and large sample kinetic rate constant values are
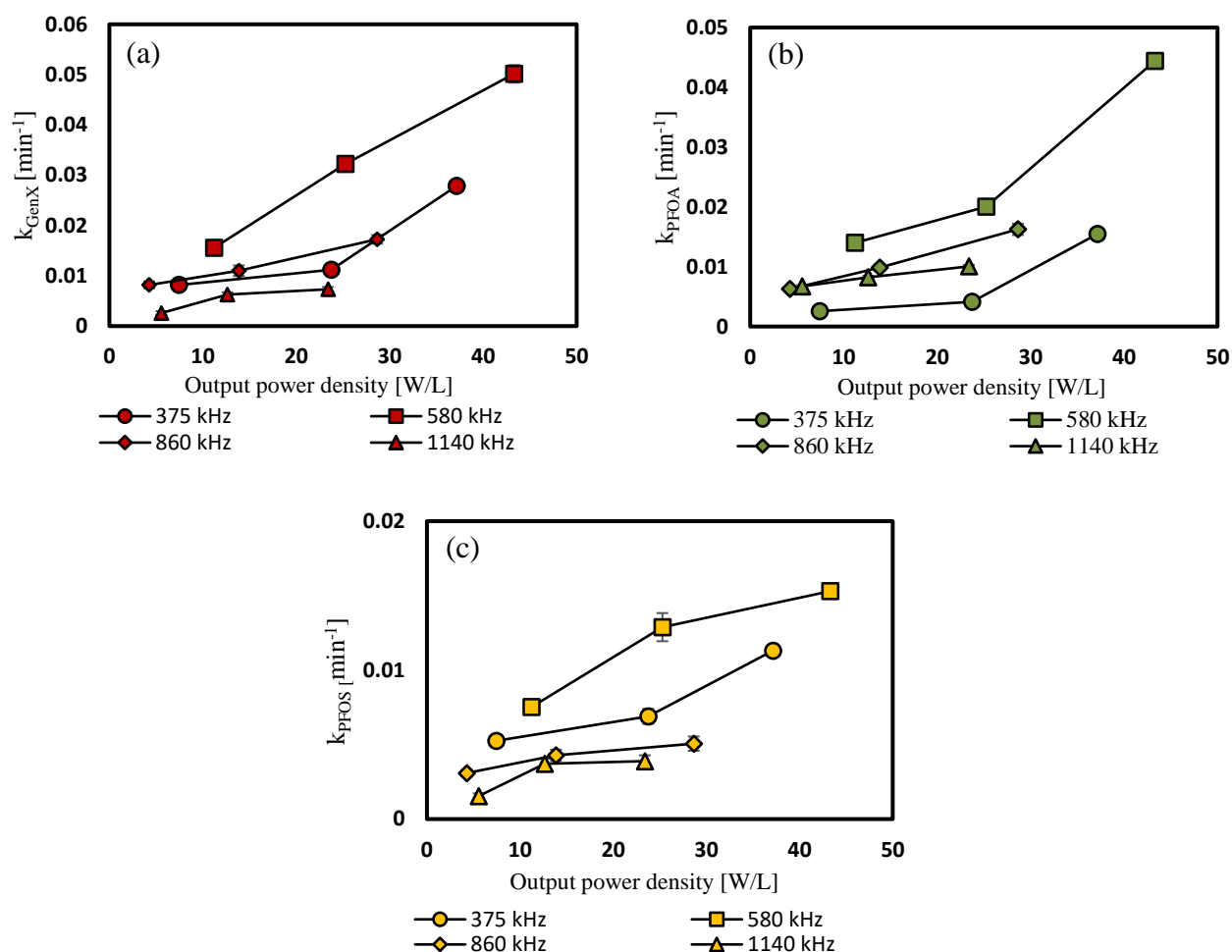368   provided in the supporting information (Figure S7 and Table S13, respectively).
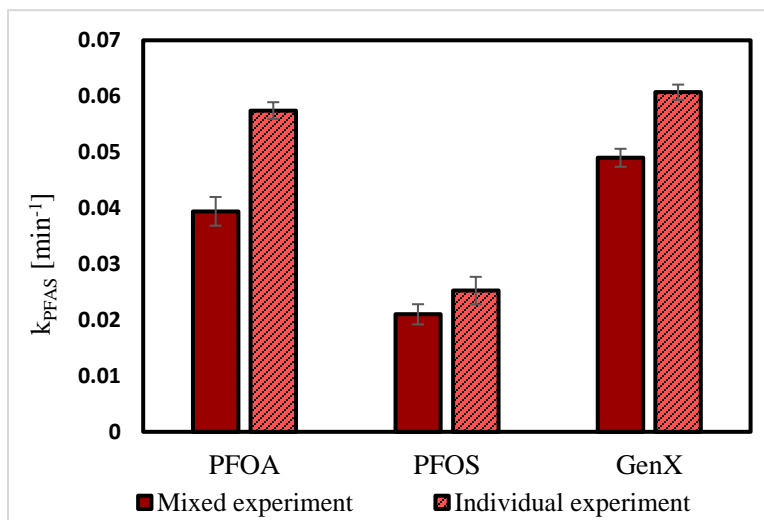


**Figure 3.** Degradation rate constant comparison between individual and mixture experiments for PFOA, PFOS, and GenX. Based on large sample kinetics The error bars represent standard errors for the degradation rate constants obtained from the LINEST function in excel.

369   A 31% reduction in degradation rate is observed for PFOA, 17% for PFOS and 19% for GenX in
370   the experiments with the PFAS mixture. Reduced overall degradation performance is expected at
371   higher initial concentrations due to a finite amount of available thermal energy in a bubble collapse
372   event, which also hints at issues with degradation efficiency in highly contaminated water
373   matrices, either due to thermal energy limitations, or due to species competing for sites on the
374   bubble interface[46].

375   The smallest reduction in performance that was observed for PFOS can be attributed to the much
376   higher bubble surface activity of PFOS compared to PFOA[47]. No study on surface activity of GenX
377   was found in literature, but if surface activity is the main driver of the observed variations, we can
378   place the surface activity of GenX as lower than that of PFOS and higher than that of PFOA.

**3.2. Output power as a measure of degradation performance**

380   The calorimetric efficiency trends observed in Figure 1 bring to question whether the calorimetric
381   efficiency is the underlying reason for the changes in degradation efficiency we observed at
382   different settings. To evaluate this, we plotted the degradation rate constants determined for GenX,
383   PFOA, and PFOS against the calorimetry-determined output power (Table S11) in Figure 4.

**Figure 4.** Degradation rate constants for (a) GenX, (b) PFOA, and (c) PFOS plotted against the output power calculated using the determined calorimetric efficiencies of the reactor at different operational settings. The error bars represent standard errors for the degradation rate constants obtained from the LINEST function in excel. If not visible, calculated error bars were smaller than the corresponding data point symbol.

Different trends are observed depending on the PFAS, apart from 375 kHz where a rising trend is apparent for all three PFAS. While 580 kHz displays a steady increase in degradation rate with GenX, a rising trend is observed for PFOA while the increase in degradation rate for PFOS declines. We can therefore claim (albeit with limitations) that the degradation efficiency for PFAS at a specific frequency directly correlates to the thermal energy introduced to the treated solution and therefore to the power applied, and more importantly, it is dependent on the calorimetric efficiency of the reactor at the given settings. The relationships between the degradation rate and calorimetric energy inputs however require further understanding. We recommend reporting reactor calorimetric efficiencies in future work for easier harmonization of experimental data and further insight into the relationship between calorimetric and degradation efficiency.

14

## 3.3. Treatment energy efficiency per order of degradation

Critically assessing advanced oxidation processes (AOPs) for their feasibility, operation costs and sustainability has been a long-standing issue in the community. The electrical energy per order ($E_{EO}$) was recommended (and accepted by IUPAC in 2001[48]) as a figure of merit for easier comparison of electrical-driven AOPs. It is defined as the electrical energy in kWh required to degrade a contaminant C by one order of magnitude in 1 m$^3$ of contaminated water[49], which in our case is obtained by multiplying the time required to achieve 90% degradation at each operational settings (calculated using the degradation rate constants) with the measured power input ($P_{input}$) of the system. When corrected for units and batch volume, we obtain Equation 5 for calculating the $E_{EO}$ in our experiments:

$$E_{EO} = \frac{\frac{\ln 0.1}{-k_{PFAS}} \times P_{input}}{30} \qquad \text{Equation 5}$$

Certain conditions need to be met for accurate comparison of $E_{EO}$ values between various AOPs[50], such as initial contaminant concentrations greater than 1 mg/L, and certainty that the operational parameters are optimized. In this study, the $E_{EO}$ values were used to assess the implied treatment costs at the various settings and were therefore calculated for all applied frequency-power settings and presented in Table 2. Note that energy data are derived from comparably inefficient lab-scale experiments and substantial improvement can be expected from reactor and transducer optimization.

**Table 2.** Electrical energy $E_{EO}$ required to degrade initial PFAS by one order of magnitude based on grid power consumption and obtained degradation kinetics at different frequencies and power densities.

| $E_{EO}$ [kWh/m$^3$] | Applied power density [W/L] | Frequency [kHz] | | | |
|---|---|---|---|---|---|
| | | 375 | 580 | 860 | 1140 |
| **GenX** | 200 | 2144 | 1129 | 2140 | 7033 |
| | 300 | 1914 | 678 | 1942 | 3477 |
| | 400 | 882 | 502 | 1490 | 3460 |
| **PFOA** | 200 | 6833 | 1258 | 2791 | 2713 |
| | 300 | 5161 | 1092 | 2165 | 2661 |
| | 400 | 1587 | 567 | 1582 | 2521 |
| **PFOS** | 200 | 3337 | 2340 | 5671 | 11763 |
| | 300 | 3102 | 1697 | 4997 | 5891 |
| | 400 | 2172 | 1644 | 5079 | 6510 |

419  Of the 3 PFAS, GenX displays the lowest energy requirements for treatment at optimal settings
420  (followed closely by PFOA). We observe a 14-fold difference between the most and least efficient
421  settings for GenX degradation. With pseudo-first order degradation of contaminants, the energy
422  consumption scales with the treatment requirements such as orders of magnitude reduction,
423  emphasizing the need for optimization of ultrasonic operation and inclusion of pre-treatment
424  before large-scale implementation and any techno-economic feasibility study.

425  As expected, energy requirements at optimum settings are approximately three orders of
426  magnitude higher than reported $E_{EO}$ values for established ozone- and UV-based AOPs (<1
427  kWh/m$^3$)[50]. This comparison is misleading however, since the literature $E_{EO}$ values are determined
428  for removal of other chemicals and most AOPs are not capable of efficiently removing PFAS[51].
429  Interestingly, our calculated $E_{EO}$ values under optimum conditions (580 kHz, 400 W/L) are at the
430  lower range of reported $E_{EO}$ values for AOPs and ARPs reported to effectively degrade PFAS. In
431  the review by Nzeribe et al. (2019)[10], $E_{EO}$ values were presented for several processes.
432  Electrochemical oxitadion for example is reported to degrade PFOA and PFOS with an energy
433  demand of 132 and 500 kWh/m$^3$, respectively. $E_{EO}$ values for ultrasonic degradation were also
434  reported, with an energy demand of ~5,000 kWh/m$^3$ for PFOA and ~20,000 kWh/m$^3$ for PFOS.
435  These values are an order of magnitude greater than the reported values in this study (567 kWh/m$^3$
436  for PFOA and 1,644 kWh/m$^3$ for PFOS). Considering that the high energy demand has been one
437  of the main arguments against using sonolysis for PFAS treatment, these findings bring ultrasonic
438  degradation of PFAS a lot closer to the economics of other AOPs and ARPs and challenge the
439  argument against using ultrasound to treat PFAS at a larger scale.

**3.4. Fluorine mass balance as an indicator of by-product formation**

441  PFAS transform into inorganic constituents $F^-$, $SO_4^{2-}$, $CO$, and $CO_2$ as a product of their complete
442  sonolytic decomposition (a.k.a. complete mineralization). Therefore, fluorine mass balance
443  experiments are conducted for all three PFAS at 580 kHz and 400 W/L. As we did not track all
444  mineralization products, but rather just the inorganic fluoride, we refer to the release of fluorine
445  from parent PFAS as defluorination rather than mineralization in further text. Both individual and
446  mixture PFAS degradation kinetics, alongside fluoride generation kinetics, were obtained from
447  large sample experiments. Firstly, we calculate the total organic fluorine content in the batch from
448  the initial PFAS concentrations, which we then compare to the sum of 1) PFAS-bound fluorine
449  (i.e. remaining total organic fluorine) calculated from the measured PFAS concentrations, and 2)
450  measured free fluoride ions in the sample at each time interval. The difference between the two
451  values indicates the presence of unknown fluorinated byproducts. According to the meta-analysis
452  by Sidnell et al.[28] , fluorine containing gases are unlikely to be the reason for discrepancies, and
453  we can thus interpret any change in ratio between the initial total organic fluorine and the fluorine
454  sum as formation of stable fluorinated species that remain in the water and are not susceptible to
455  further ultrasonic degradation.

456  Therefore, we can use the fluorine mass balance to assess how efficiently each of the three PFAS
457  defluorinates. Figure 5 represents the GenX degradation kinetics with a fluorine mass balance. The
458  data for PFOA and PFOS can be found in Figure S9 of the SI.
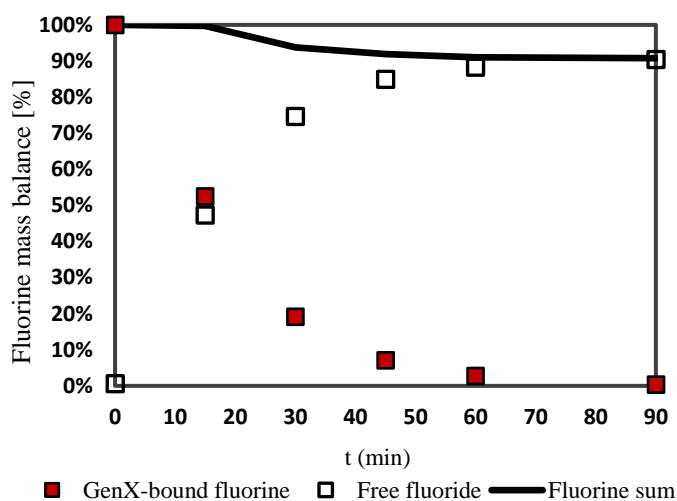
459  **Figure 5.** GenX fluorine mass balance as a function of time at 580 kHz and 400 W/L.
460  Data obtained from large sample volume experiments.

461  While the relative degradation kinetics between different PFAS are in line with the other
462  experiments, absolute kinetics are slightly increased compared to experiments with small sample
463  volumes due to changes in batch volume caused by sampling. In the large sampling experiments,
464  GenX degraded bellow the limit of detection after 90 minutes, while 99% of PFOA and 90% of
465  PFOS degraded in the same time frame. However, defluorination efficiency and thus unknown
466  byproduct formation vary greatly between the three PFAS. After 90 minutes, we account for 90%
467  of initial total organic fluorine in the case of GenX indicating a very efficient cleavage of C-F
468  bonds with little formation of stable byproducts. During sonolysis of PFOA and PFOS, the fluorine
469  sum was lower in the final sample (mass balance was closed by 76% and 70%, respectively). The
470  defluorination rate observed is higher than for many other reported methods (ranging from 0-80%
471  defluorination)[10]. Furthermore, we observe that byproduct formation and loss of fluorine (i.e.
472  deviation from 100% sum) in the mass balance occurs quickest with PFOA and slowest with
473  PFOS. With the degradation mechanism discussed in chapter 3.1.1. in mind, where sonolytic
474  degradation of PFAS occurs through headgroup cleavage and/or immediate pyrolysis of the PFAS
475  species, we postulate that due to its lower thermal stability, GenX defluorinates most efficiently
476  while PFOS generates the highest amount of unknown fluorinated species over time due to higher
477  thermal resistance and therefore incomplete pyrolysis during cavitation events.

478  Since no expected by-products (predicted based on the truncation mechanism and covered in our
479  LC-MS/MS method) were detected in the samples, it is most likely that stable unknown fluorinated
480  species form immediately during the pyrolytic mineralization of all three PFAS, rather than
481  through gradual defluorination of a series of intermediates.

482  In addition to full fluoride kinetics obtained at 580 kHz and 400 W/L, final mineralization data
483  was obtained for all settings from small sample experiments using the final sample of each
484  experimental run, which was always stored in sufficient volume. The percentages of degraded and
485  fully defluorinated PFAS at all tested powers and frequencies are presented in the supporting
486  information (Figure S8). While the degradation of PFAS increased consistently with power, no

487 such trend was observed with defluorination efficiency, where the rate of defluorination varied
488 with no obvious influence of frequency or power. The amount of fluorine in unknown fluorinated
489 by-products, however, never exceeded 30% of total organic fluorine, regardless of the degradation
490 performance at those settings.

### 3.4.1. Mineralization performance in mixture experiments

491
492 A fluorine mass balance was also measured for a mixture experiment, to observe if defluorination
493 efficiencies obtained from individual experiments can be transferred into a mixture degradation
494 experiment. Since the ion-selective electrode only provides a cumulative fluoride concentration,
495 the removal of PFAS obtained in LC/MS-MS measurements was used to calculate a theoretical
496 maximum release of total organic fluorine if we assume 100% defluorination. This theoretical
497 release from individual PFAS was cumulated to determine the PFAS-based maximum, and the
498 difference to the measured fluoride represents formation of stable fluorinated species. The actual
499 defluorination of individual PFAS in the mixture experiment was estimated by correcting the
500 quantified PFAS removal at different time intervals using the defluorination efficiencies at
501 different time intervals obtained from individual experiments described in chapter 3.4. Figure 6
502 displays the measured fluoride concentration at each time interval, the maximum expected fluoride
503 concentration based on LC/MS-MS data, and individual fluoride estimates based on individual
504 defluorination efficiency data.
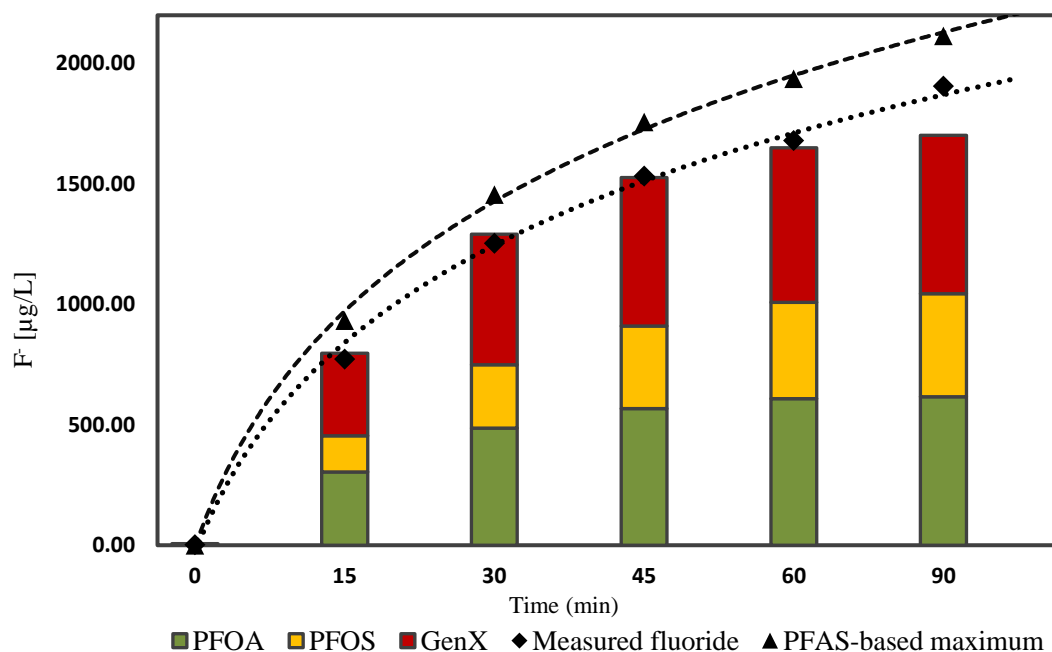


**Figure 6.** Mixture experiment fluorine mass balance. A theoretical maximum release of
total organic fluorine is calculated from the quantified PFAS removal and cumulated into
a PFAS-based maximum. The difference to the measured fluoride represents formation of
stable fluorinated species. The actual defluorination of individual PFAS in the mixture
was estimated by correcting the quantified PFAS removal at different time intervals using
the observed defluorination efficiency at different time intervals during individual fluorine
mass balance experiments.

513    The fluoride concentration estimates based on defluorination efficiency fit the measured fluoride
514    values well, implying that individual defluorination efficiency is transferable into mixed PFAS
515    matrices. Only at minute 90 we observed a higher measured fluoride concentration than the
516    predicted one, presumably due to higher total PFAS presence at minute 90 compared to individual
517    experiments. We can thus conclude that defluorination of PFAS spoken in general terms occurs
518    more efficiently at higher total PFAS concentrations.

519

## 4. Conclusions and outlook

521    Conducted experiments revealed that with the increase in applied power density, the degradation
522    rate of PFAS increases consistently within a single frequency. However, this increase is not equal
523    at all frequencies. Among 375, 580, 860 and 1,140 kHz, the 580 kHz frequency displayed the
524    highest degradation performance for all three PFAS tested. While all three PFAS degrade quickest
525    at 580 kHz, we observed 375 kHz as the second-best frequency for PFOS, whereas the 860 kHz
526    frequency acts as the second-best for PFOA. GenX degraded equally at 375 kHz and 860 kHz,
527    only showing preference for 375 kHz at the highest power density.

528    The LC-MS/MS method for the analysis of PFAS was developed to include both the parent PFAS
529    and the expected by-products of the truncation mechanism. No formation of known by-products
530    was observed in our experimental samples indicating that the degradation of the tested PFAS
531    occurs through immediate and (in-)complete pyrolysis of parent PFAS species during bubble
532    collapse events. Regardless, fluorine mass balance experiments at optimal settings revealed some
533    loss of fluorine. Per literature reports, fluorine-containing gases are unlikely to be the reason for
534    discrepancies, but rather the formation of stable unknown fluorinated species that remain in the
535    treated solution. At the optimal settings of 580 kHz and 400 W/L, GenX degrades and defluorinates
536    most efficiently among the three tested PFAS, while PFOS degrades with lowest efficiency. The
537    observed difference at optimal settings is in direct agreement with the literature-reported thermal
538    stability of the three species of PFAS (PFOS > PFOA > GenX), solidifying the statement that
539    thermolysis plays a major role in the sonolytic degradation of PFAS.

540    When degrading GenX, PFOA and PFOS (1 mg/L each) in a mixture, all three PFAS displayed
541    lower degradation rates (i.e., at higher total PFAS concentration) compared to experiments with
542    individual target chemicals. PFOA exhibited the largest reduction in degradation rate (by 31%),
543    followed by GenX (by 19%) and finally by PFOS (by 17%). We attribute the smallest reduction
544    in performance observed for PFOS to the higher bubble surface activity of PFOS compared to
545    PFOA, as PFOS diffuses to the bubble interface more readily. No study on the surface activity of
546    GenX has been found in the literature, but if surface activity is the main driver of the observed
547    variations, we can place the surface activity of GenX as lower than that of PFOS and higher than
548    that of PFOA.

549    Calorimetric efficiency is suggested to be reported in future work for easier harmonization of data
550    between various systems, as it directly indicates the relative amount of consumed energy that was
551    introduced to the bulk of solution as thermal energy over time. As such, it could prove as a simple

552    to determine reactor parameter that encompasses more difficult to quantify parameters and
553    phenomena that result from varying reactor geometries, distances and solid barriers between
554    transducer and sample, and similar. For this reason, determined degradation rates are reported
555    using the output power, and the community is encouraged to report the calorimetric efficiency of
556    their ultrasonic systems in the future. Treatment efficiency at different settings is evaluated using
557    the Energy per unit order ($E_{EO}$). Of the three PFAS, GenX displays the lowest energy requirements
558    for treatment at optimal settings. Although a relatively inefficient lab-scale system, the determined
559    $E_{EO}$ values are already in the range of reported $E_{EO}$ values for other AOPs and ARPs, and an order
560    of magnitude lower than reported energy requirements for ultrasonic treatment of PFOA and
561    PFOS. Through optimization and further understanding of the process, ultrasonic cavitation could
562    rise to first place as a robust, easy-to-use, no-additives method for treating highly contaminated
563    PFAS streams.

564

565 **CRediT authorship contribution statement**

566 **Nebojša Ilić:** Conceptualization, Investigation, Data curation, Visualization, Formal analysis,
567 Writing – original draft preparation. **Afrina Andalib:** Investigation, Data curation, Writing –
568 original draft preparation. **Thomas Lippert:** Conceptualization, Investigation, Writing –
569 reviewing and editing. **Oliver Knoop:** Conceptualization, Writing – reviewing and editing,
570 Analytical support. **Marcus Franke:** Conceptualization, Writing – reviewing and editing. **Patrick**
571 **Bräutigam:** Writing – reviewing and editing. **Jörg E. Drewes:** Funding acquisition, writing –
572 reviewing and editing. **Uwe Hübner:** Conceptualization, Writing – reviewing and editing,
573 Supervision.

574

575 **Declaration of Competing Interest**

576 The authors declare that they have no known competing financial interests or personal
577 relationships that could have appeared to influence the work reported in this paper.

578

579 **Acknowledgments**

583

## References

585  1.  Buck, R. C. *et al.* Perfluoroalkyl and polyfluoroalkyl substances in the environment:
586      terminology, classification, and origins. *Integr Environ Assess Manag* **7**, 513–541 (2011).

587  2.  Wang, Z., DeWitt, J. C., Higgins, C. P. & Cousins, I. T. A Never-Ending Story of Per- and
588      Polyfluoroalkyl Substances (PFASs)? *Environ Sci Technol* **51**, 2508–2518 (2017).

589  3.  Cordner, A. *et al.* Guideline levels for PFOA and PFOS in drinking water: the role of
590      scientific uncertainty, risk assessment decisions, and social factors. *J Expo Sci Environ*
591      *Epidemiol* **29**, 157–171 (2019).

592  4.  Sun, M. *et al.* Legacy and Emerging Perfluoroalkyl Substances Are Important Drinking
593      Water Contaminants in the Cape Fear River Watershed of North Carolina. *Environ Sci*
594      *Technol Lett* **3**, 415–419 (2016).

595  5.  Joerss, H. *et al.* Per- and polyfluoroalkyl substances in Chinese and German river water –
596      Point source- and country-specific fingerprints including unknown precursors.
597      *Environmental Pollution* **267**, 115567 (2020).

598  6.  Sahu, S. P. *et al.* Rapid Degradation and Mineralization of Perfluorooctanoic Acid by a New
599      Petitjeanite Bi 3 O(OH)(PO 4 ) 2 Microparticle Ultraviolet Photocatalyst. *Environ Sci*
600      *Technol Lett* **5**, 533–538 (2018).

601  7.  Zhang, Z., Chen, J.-J., Lyu, X.-J., Yin, H. & Sheng, G.-P. Complete mineralization of
602      perfluorooctanoic acid (PFOA) by γ-irradiation in aqueous solution. *Sci Rep* **4**, 7418 (2014).

603  8.  Zhuo, Q., Deng, S., Yang, B., Huang, J. & Yu, G. Efficient electrochemical oxidation of
604      perfluorooctanoate using a Ti/SnO2-Sb-Bi anode. *Environ Sci Technol* **45**, 2973–2979
605      (2011).

606  9.  Yang, L.-H. *et al.* Is HFPO-DA (GenX) a suitable substitute for PFOA? A comprehensive
607      degradation comparison of PFOA and GenX via electrooxidation. *Environ Res* **204**, 111995
608      (2022).

609  10. Nzeribe, B. N., Crimi, M., Mededovic Thagard, S. & Holsen, T. M. Physico-Chemical
610      Processes for the Treatment of Per- And Polyfluoroalkyl Substances (PFAS): A review. *Crit*
611      *Rev Environ Sci Technol* **49**, 866–915 (2019).

612  11. Pinkard, B. R., Shetty, S., Stritzinger, D., Bellona, C. & Novosselov, I. V. Destruction of
613      perfluorooctanesulfonate (PFOS) in a batch supercritical water oxidation reactor.
614      *Chemosphere* **279**, 130834 (2021).

615  12. Stratton, G. R. *et al.* Plasma-Based Water Treatment: Efficient Transformation of
616      Perfluoroalkyl Substances in Prepared Solutions and Contaminated Groundwater. *Environ*
617      *Sci Technol* **51**, 1643–1648 (2017).

618  13.  Suslick, K. S., Doktycz, S. J. & Flint, E. B. On the origin of sonoluminescence and
619      sonochemistry. *Ultrasonics* **28**, 280–290 (1990).

620  14.  Oturan, M. A. & Aaron, J.-J. Advanced Oxidation Processes in Water/Wastewater
621      Treatment: Principles and Applications. A Review. *Crit Rev Environ Sci Technol* **44**, 2577–
622      2641 (2014).

623  15.  Suslick, K. S. Sonochemistry. *Science (1979)* **247**, 1439–1445 (1990).

624  16.  Kanthale, P., Ashokkumar, M. & Grieser, F. Sonoluminescence, sonochemistry (H2O2
625      yield) and bubble dynamics: frequency and power effects. *Ultrason Sonochem* **15**, 143–150
626      (2008).

627  17.  Tronson, R., Ashokkumar, M. & Grieser, F. Multibubble Sonoluminescence from Aqueous
628      Solutions Containing Mixtures of Surface Active Solutes. *J Phys Chem B* **107**, 7307–7311
629      (2003).

630  18.  Chiha, M. *et al.* Modeling of ultrasonic degradation of non-volatile organic compounds by
631      Langmuir-type kinetics. *Ultrason Sonochem* **17**, 773–782 (2010).

632  19.  Vecitis, C. D., Park, H., Cheng, J., Mader, B. T. & Hoffmann, M. R. Kinetics and
633      mechanism of the sonolytic conversion of the aqueous perfluorinated surfactants,
634      perfluorooctanoate (PFOA), and perfluorooctane sulfonate (PFOS) into inorganic products.
635      *J Phys Chem A* **112**, 4261–4270 (2008).

636  20.  Javed, H., Lyu, C., Sun, R., Zhang, D. & Alvarez, P. J. J. Discerning the inefficacy of
637      hydroxyl radicals during perfluorooctanoic acid degradation. *Chemosphere* **247**, 125883
638      (2020).

639  21.  Venkatesan, A. K., Lee, C.-S. & Gobler, C. J. Hydroxyl-radical based advanced oxidation
640      processes can increase perfluoroalkyl substances beyond drinking water standards: Results
641      from a pilot study. *Science of The Total Environment* **847**, 157577 (2022).

642  22.  Beckett, M. A. & Hua, I. Impact of Ultrasonic Frequency on Aqueous Sonoluminescence
643      and Sonochemistry. *Journal of Physical Chemistry A* **105**, 3796–3802 (2001).

644  23.  Petrier, C. & Francony, A. Incidence of wave-frequency on the reaction rates during
645      ultrasonic wastewater treatment. *Water Science and Technology* **35**, 175–180 (1997).

646  24.  Ciawi, E., Rae, J., Ashokkumar, M. & Grieser, F. Determination of temperatures within
647      acoustically generated bubbles in aqueous solutions at different ultrasound frequencies. *J
648      Phys Chem B* **110**, 13656–13660 (2006).

649  25.  Barber, Wu, Löfstedt, Roberts & Putterman. Sensitivity of sonoluminescence to
650      experimental parameters. *Phys Rev Lett* **72**, 1380–1383 (1994).

651  26.  Thompson, L. H. & Doraiswamy, L. K. Sonochemistry: Science and Engineering. *Ind Eng
652      Chem Res* **38**, 1215–1249 (1999).

653    27.    Koda, S., Kimura, T., Kondo, T. & Mitome, H. A standard method to calibrate
654         sonochemical efficiency of an individual reaction system. *Ultrason Sonochem* **10**, 149–156
655         (2003).

656    28.    Sidnell, T., Wood, R. J., Hurst, J., Lee, J. & Bussemaker, M. J. Sonolysis of per- and poly
657         fluoroalkyl substances (PFAS): A meta-analysis. *Ultrason Sonochem* **87**, 105944 (2022).

658    29.    Campbell, T. & Hoffmann, M. R. Sonochemical degradation of perfluorinated surfactants:
659         Power and multiple frequency effects. *Sep Purif Technol* **156**, 1019–1027 (2015).

660    30.    Wood, R. J. *et al.* Ultrasonic degradation of perfluorooctane sulfonic acid (PFOS) correlated
661         with sonochemical and sonoluminescence characterisation. (2019)
662         doi:10.13140/RG.2.2.36006.88645.

663    31.    Rodriguez-Freire, L., Balachandran, R., Sierra-Alvarez, R. & Keswani, M. Effect of sound
664         frequency and initial concentration on the sonochemical degradation of perfluorooctane
665         sulfonate (PFOS). *J Hazard Mater* **300**, 662–669 (2015).

666    32.    Rodriguez-Freire, L. *et al.* Sonochemical degradation of perfluorinated chemicals in
667         aqueous film-forming foams. *J Hazard Mater* **317**, 275–283 (2016).

668    33.    Asakura, Y. & Yasuda, K. Frequency and power dependence of the sonochemical reaction.
669         *Ultrason Sonochem* **81**, 105858 (2021).

670    34.    Mason, T. J. & Lorimer, J. P. *Applied sonochemistry*. (Wiley-VCH, 2002).
671         doi:10.1002/352760054X.

672    35.    Jiang, Y., Pétrier, C. & David Waite, T. Kinetics and mechanisms of ultrasonic degradation
673         of volatile chlorinated aromatics in aqueous solutions. *Ultrason Sonochem* **9**, 317–323
674         (2002).

675    36.    Gutierrez, Maritza. & Henglein, Arnim. Chemical action of pulsed ultrasound: observation
676         of an unprecedented intensity effect. *J Phys Chem* **94**, 3625–3628 (1990).

677    37.    Nebojša Ilić. Ultrasound-driven degradation data for GenX, PFOA and PFOS at different
678         ultrasonic frequencies and power densities. Preprint at (2023).

679    38.    Moriwaki, H. *et al.* Sonochemical decomposition of perfluorooctane sulfonate and
680         perfluorooctanoic acid. *Environ Sci Technol* **39**, 3388–3392 (2005).

681    39.    Fernandez, N. A., Rodriguez-Freire, L., Keswani, M. & Sierra-Alvarez, R. Effect of
682         chemical structure on the sonochemical degradation of perfluoroalkyl and polyfluoroalkyl
683         substances (PFASs). *Environ Sci (Camb)* **2**, 975–983 (2016).

684    40.    O'Hagan, D. Understanding organofluorine chemistry. An introduction to the C-F bond.
685         *Chem Soc Rev* **37**, 308–319 (2008).

686    41.    Franklin, J. L. & Lumpkin, H. E. Some C-S, H-S and S-S Bond Strengths by the Electron
687         Impact Method. *J Am Chem Soc* **74**, 1023–1026 (1952).

688  42.  Bentel, M. J. *et al.* Defluorination of Per- and Polyfluoroalkyl Substances (PFASs) with
689        Hydrated Electrons: Structural Dependence and Implications to PFAS Remediation and
690        Management. *Environ Sci Technol* **53**, 3718–3728 (2019).

691  43.  Shende, T., Andaluri, G. & Suri, R. P. S. Kinetic model for sonolytic degradation of non-
692        volatile surfactants: Perfluoroalkyl substances. *Ultrason Sonochem* **51**, 359–368 (2019).

693  44.  Xiao, F. *et al.* Thermal Stability and Decomposition of Perfluoroalkyl Substances on Spent
694        Granular Activated Carbon. *Environ Sci Technol Lett* **7**, 343–350 (2020).

695  45.  Sostaric, J. Z. & Riesz, P. Adsorption of Surfactants at the Gas/Solution Interface of
696        Cavitation Bubbles: An Ultrasound Intensity-Independent Frequency Effect in
697        Sonochemistry. *J Phys Chem B* **106**, 12537–12548 (2002).

698  46.  Cheng, J., Vecitis, C. D., Park, H., Mader, B. T. & Hoffmann, M. R. Sonochemical
699        Degradation of Perfluorooctane Sulfonate (PFOS) and Perfluorooctanoate (PFOA) in
700        Landfill Groundwater: Environmental Matrix Effects. *Environ Sci Technol* **42**, 8057–8063
701        (2008).

702  47.  Vecitis, C. D., Park, H., Cheng, J., Mader, B. T. & Hoffmann, M. R. Enhancement of
703        Perfluorooctanoate and Perfluorooctanesulfonate Activity at Acoustic Cavitation Bubble
704        Interfaces. *The Journal of Physical Chemistry C* **112**, 16850–16857 (2008).

705  48.  Bolton, J. R., Bircher, K. G., Tumas, W. & Tolman, C. A. Figures-of-merit for the technical
706        development and application of advanced oxidation technologies for both electric- and
707        solar-driven systems (IUPAC Technical Report). *Pure and Applied Chemistry* **73**, 627–637
708        (2001).

709  49.  Bolton, J. R., Bircher, K. G., Tumas, W. & Tolman, C. A. Figures-of-Merit for the Technical
710        Development and Application of Advanced Oxidation Processes. *Journal of Advanced
711        Oxidation Technologies* **1**, (1996).

712  50.  Miklos, D. B. *et al.* Evaluation of advanced oxidation processes for water and wastewater
713        treatment – A critical review. *Water Res* **139**, 118–131 (2018).

714  51.  Dombrowski, P. M. *et al.* Technology review and evaluation of different chemical oxidation
715        conditions on treatability of PFAS. *Remediation* **28**, 135–150 (2018).

716